Ultrathick and High-Aspect-Ratio Nickel Microgyroscope Using EFAB Multilayer Additive Electroforming

Said Emre Alper, Ilker Ender Ocak, and Tayfun Akin, *Member, IEEE*

***Abstract*—This paper presents a new approach for the development of a microgyroscope that has a 240-μm-thick multilayer electroformed-nickel structural mass and a lateral aspect ratio greater than 100. The gyroscope is fabricated using commercial multilayer additive electroforming process EFAB of Microfabrica, Inc., which allows defining the thickness of different structural regions, such as suspensions, proof mass, and capacitive electrodes, unlike many classical surface-micromachining technologies that require a uniform thickness for the structural features. The capacitive gaps of the gyroscope are designed to be laying parallel to the substrate plane and can be set as small as 4 μm, and therefore, the lateral aspect ratio, which is defined as the ratio of the overlap length of capacitor plates to the gap spacing, can easily exceed 100. The high capacitive aspect ratio, multilayer capacitors, and thick proof mass altogether yield a highly sensitive gyroscope for in-plane angular-rate measurements. Characterization of the fabricated gyroscope using a very simple capacitive interface circuit constructed from standard IC components yields a measured mechanical sensitivity of 65 μV/(°/s) and a noise equivalent rate of 0.086 °/s at atmospheric pressure in a bandwidth of 1 Hz. The response bandwidth is limited to 100 Hz when the resonance frequencies of the drive and sense modes are matched by electrostatic tuning. The measured stability of the drive-mode resonance frequency is better than 0.1% within a 40-h period, demonstrating reliability of electroformed nickel of EFAB process. In addition, the mechanical quality factor of the sense mode reaches 2000 at 20-mtorr vacuum, verifying the quality of structural nickel. The resonance-frequency variations of the drive and sense modes with respect to increasing temperature are characterized to be smaller than 1 and -2 Hz/°C, respectively, in the -40-°C to $+85$-°C measurement range. The gyroscope performance can be further increased by reducing the minimum capacitive gaps, by increasing the number of stacked layers, by using a nickel–alloy structural layer with better mechanical properties, and by using a dedicated CMOS–application-specified integrated circuit which are under consideration. [2006-0275]**

***Index Terms*—Angular-rate sensor, electroformed gyroscope, gyroscope, multilayer electroforming.**

Manuscript received December 11, 2006; revised June 5, 2007. This paper was presented at the 19th IEEE International Conference on Microelectromechanical Systems (MEMS 2006), Istanbul, Turkey, January 2006. Subject Editor R. Howe.

The authors are with the Department of Electrical and Electronics Engineering, Middle East Technical University, 06531 Ankara, Turkey (e-mail: said@metu.edu.tr; ocak@mems.eee.metu.edu.tr; tayfun-akin@metu.edu.tr).

Color versions of one or more of the figures in this paper are available online at http://ieeexplore.ieee.org.

Digital Object Identifier 10.1109/JMEMS.2007.902431

I. Introduction

MEMS gyroscopes have attracted a lot of attention in the past decade for applications requiring low-cost and compact-size gyroscopes with rate- to tactical-grade performance, such as automotive safety systems, industrial stabilization, and some military applications. The cost, compactness, and accuracy of these gyroscopes are typically dominated by the limited integration capability of MEMS processes with CMOS electronics and the necessity of sealing the tiny mechanical components of MEMS gyroscopes in a vacuum ambient. Without a vacuum ambient, the performance of these gyroscopes is greatly limited due to gas-damping effects. Development of MEMS gyroscopes with CMOS integration capability and operation at atmospheric pressure levels without compromising the performance requirements is desirable for realization of truly low-cost, compact, and reliable angular-rate sensing systems.

The high aspect-ratio micromachining capability [1], [2], the superior mechanical properties of silicon over metals [2], and the variety of silicon-micromachining technologies [1]–[7] increased the popularity of silicon gyroscopes against electroformed-metal gyroscopes. A variety of silicon-micromachining technologies allow high sensitivity of out-of-plane microgyroscopes using bulk-micromachining technology [1] or of in-plane gyroscopes using silicon surface-micromachining technology [5]. There are also approaches for combining surface and bulk micromachining [8], which can be considered for fabricating out-of-plane and in-plane gyroscopes on the same substrate. However, the high complexity, low yield, low throughput, and resulting high cost of these technologies make them weak candidate for realization. Besides that, monolithic integration of silicon-micromachining technologies with CMOS processes is difficult, which requires hybrid integration of the gyroscopes and CMOS electronics, which limits the performance and increases the packaging costs. Still, an alternative approach for the production of smart gyroscopes integrated with readout electronics is metal-electroforming technology. Unfortunately, there is no significant progress reported for electroformed microgyroscopes, which is primarily due to the limited aspect ratio of electroforming processes, the low-quality factor of electroformed nickel even at vacuum, and the reliability issues for the nickel structural material. The gyroscopes fabricated using standard nickel-electroforming processes with standard photoresist sacrificial molds result to an aspect ratio that is limited to a maximum of 2–3, yielding rate-grade

performance ($> 0.1\ ^\circ/\mathrm{s}$) [9], [10] even at vacuum. It is possible to improve the performance of the electroformed gyroscopes by employing symmetric and decoupled structures fabricated with thick photoresist molds [11], achieving aspect ratios above seven, which is typically the limit of standard UV lithography. Still, the performance of these gyroscopes is limited to $0.05\ ^\circ/\mathrm{s}$ at vacuum ambient and to $0.1\ ^\circ/\mathrm{s}$ at atmospheric pressure. Another nickel gyroscope in a lithographie galvanoformung abformung (LIGA) process is reported with an aspect ratio greater than 25, yielding a noise equivalent rate better than $0.04\ ^\circ/\mathrm{s}$ at vacuum operation [12]; however, LIGA is a nonstandard and expensive process, and it is known to create problems during CMOS integration. It would be impressive to develop an electroformed gyroscope yielding a high sensitivity even at atmospheric pressure and fabricated in a low-cost, CMOS-compatible, and standard electroforming process.

This paper reports for the first time a decoupled in-plane gyroscope [13] is fabricated through additive stacking of a number of structural nickel layers using a standard electroforming process EFAB developed by Microfabrica, Inc. The fabricated gyroscope has high aspect-ratio capacitive gaps providing high sensitivity, submillimeter-thick proof mass reducing thermomechanical noise, decoupled drive and sense modes for minimizing mechanical crosstalk, and high-quality factors even at atmospheric pressure, which yield remarkable performance even without a need for vacuum. The gyroscope is designed for in-plane angular-rate measurements, and therefore, the presented approach is also attractive for dual-axis rate-sensing applications using two high-performance in-plane rate sensors fabricated on the same substrate, operating at atmospheric pressure, and fabricated through a CMOS-compatible process.

II. Electromechanical Design and Simulations

Fig. 1 shows the structure of the multilayer electroformed gyroscope, where its outer frame and inner gimbal are oscillated along the drive mode using linear comb drives. When an angular-rate input is applied about the sensitive axis of the gyroscope, the inner gimbal oscillates along the sense mode due to Coriolis effect, and the oscillation amplitude is detected with the varying-gap-type capacitive sense electrodes. Suspensions of the gyroscope are designed in such a way that the outer frame is limited to 1 degree of freedom (DOF), while the inner gimbal has 2 DOF; therefore, the outer frame and inner gimbal are decoupled from each other, preventing possible cross interaction from the sense-mode oscillations to the drive-mode oscillations [5]. The structure also includes overrange stoppers as a protection against external shock and vibrations.

The thickness of the suspensions for the drive-mode oscillating mass is set to 50 μm in order to increase the stiffness of the outer frame in out-of-plane direction. On the other hand, the suspensions for the inner sense-mode mass has a thickness of only 15 μm and a width of 30 μm, being stiff along the drive-mode oscillation direction and loose along the out-of-plane sense-mode vibration direction. Obviously, the ability to set different thicknesses for the suspension beams of the drive- and sense-mode oscillations is very useful in defining the proper

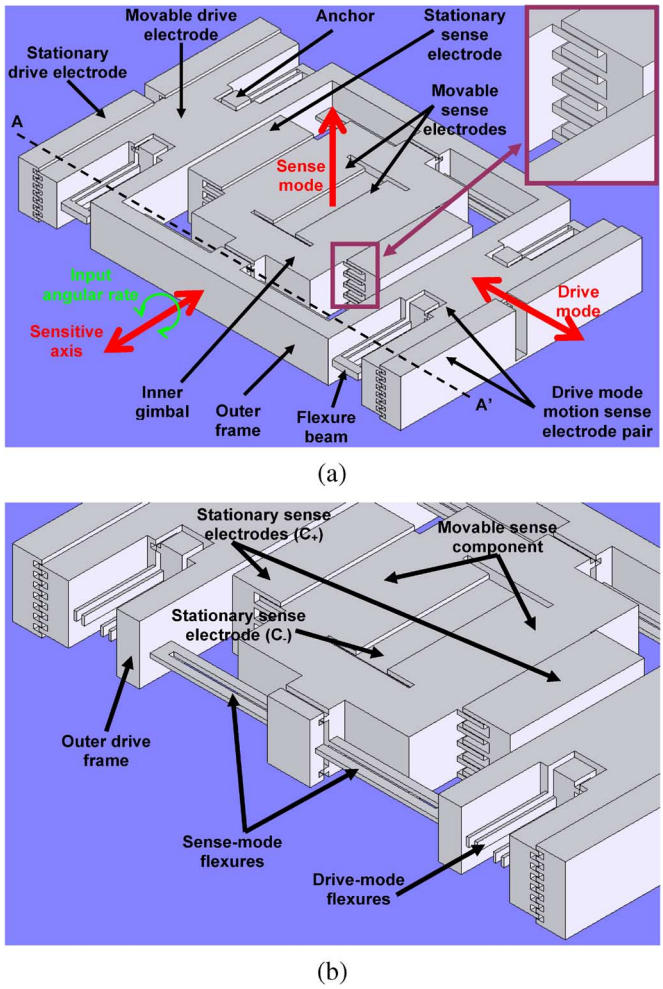

Fig. 1. Structure of the proposed gyroscope. (a) Overall view. (b) Close-up view across A–A' of (a).

DOF for different moving parts associated with drive and sense modes and is a distinctive benefit of the EFAB process, which is discussed in the next section.

Fig. 2(a) shows the drive electrode of the gyroscope, which has the structure of linear comb fingers that are stacked on top of each other, and the capacitive gaps which are parallel to the substrate surface. This structure is similar to the linear comb drives implemented in typical comb-drive resonators [14]; however, the aspect ratio of the capacitive gap, which is defined as the ratio of the overlap length of the capacitor plates to the gap spacing, can easily exceed 100 since the overlap length of these capacitors is virtually unlimited. Such a high aspect ratio cannot be achieved even by deep reactive-ion etching in silicon micromachining. On the other hand, the cost for unlimited aspect ratio of horizontal capacitors is the reduced number of comb fingers, which is limited by the number of stacked nickel layers, which is also virtually unlimited. Fig. 2(b) shows the sense electrodes of the gyroscope, having a varying-gap nature in order to maximize the rate sensitivity and to allow electrostatic frequency tuning.

Fig. 3 shows the mode shapes for the drive and sense modes of the designed gyroscope as simulated by the CoventorWare finite-element modeling (FEM) software. The

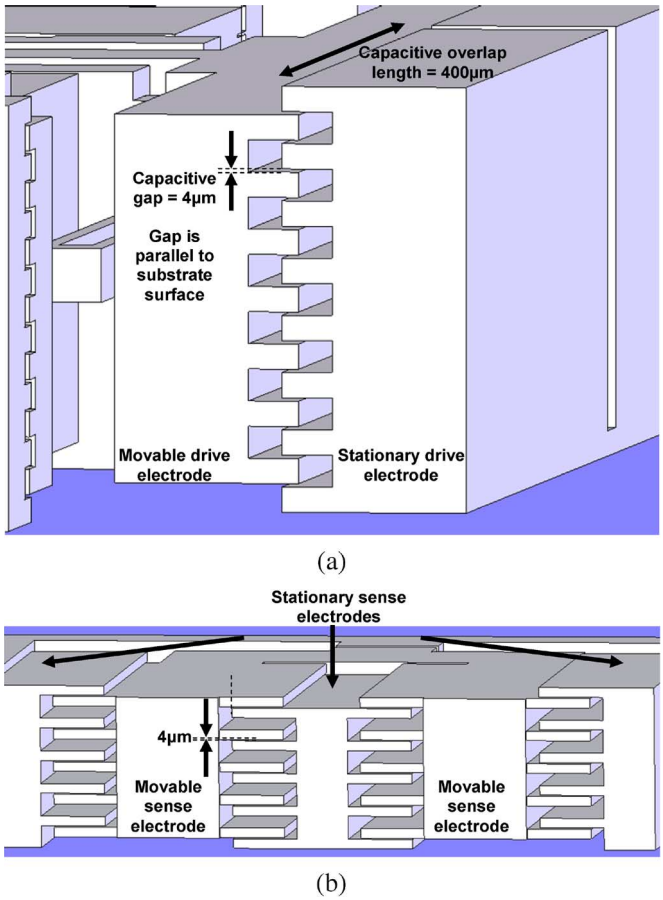

Fig. 2. Mechanical structure of (a) varying-overlap-area-type drive electrode and (b) varying-gap-type sense electrode of the designed gyroscope structure. The capacitive gaps are parallel to the substrate surface allowing a large lateral aspect ratio for the electrode capacitances.

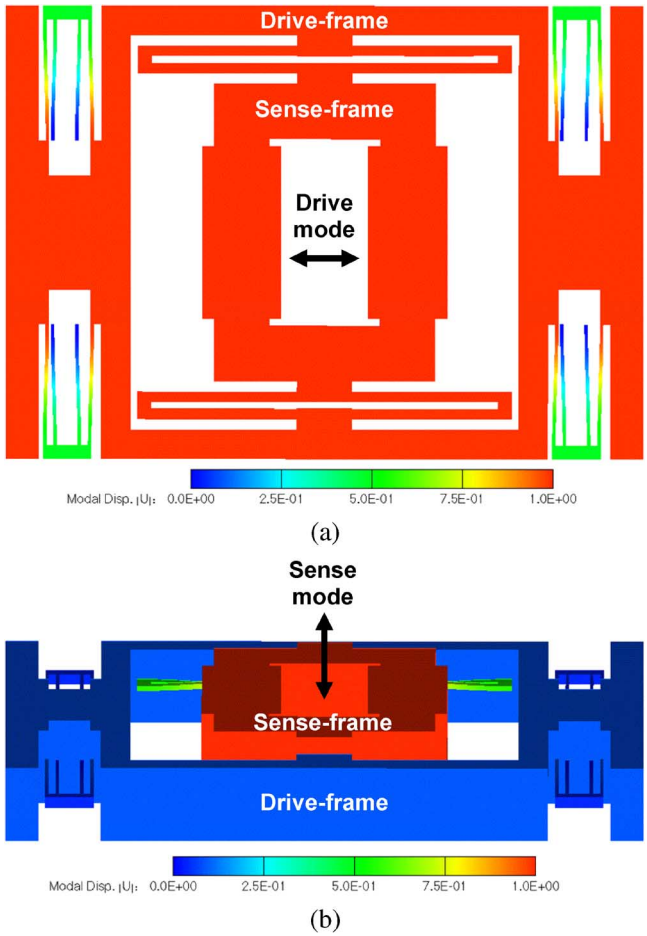

Fig. 3. FEM modal simulations performed by CoventorWare, showing the mode shapes of the (a) drive and (b) sense modes of the gyroscope.

resonance frequencies of the drive and sense modes are set as 2.41 and 3.41 kHz, respectively. In addition to the modal simulations, a stress analysis has been performed on the designed gyroscope for determining the flexure lengths and stopper locations in order to keep the maximum stress induced in the gyroscope smaller than the minimum predicted fatigue limit for electroformed nickel, which is about 100 MPa [15]. The maximum stress values appearing on the drive- and sense-mode flexures are also simulated for an external shock signal of 1000 g applied along each mode. The maximum stress values for 3-μm maximum deflection along the drive mode and 2-μm maximum deflection along the sense mode are simulated to be 73 and 87 MPa, respectively. The allowable maximum deflections are set and limited by the mechanical overrange-stopper elements. Therefore, the gyroscope is designed to be safe against large physical shocks, making it appropriate for a number of high-g environments.

III. Fabrication Process

The gyroscope is fabricated using commercially available EFAB multilayer additive electroforming process of Microfabrica, Inc. [16]. Fig. 4 shows the fabrication of a single electroformed layer as well as a sample microstructure fabricated by stacking several layers on top of each other. The process is based on electroforming a sacrificial copper layer using a hard mask, creating unplated vias, followed by electroforming nickel on the whole surface including the vias, and finally planarizing the electroformed nickel so that it only remains inside via regions. This cycle is repeated for different masks, forming one of the horizontal strips of the final structure in each step. The sacrificial copper layer is selectively etched at the end of the process, releasing the microstructures.

Fig. 5 shows the SEM pictures of the fabricated gyroscope that occupies an area of 2.1×1.3 mm^2. The gyroscope is fabricated with 31 electroformed layers reaching to a thickness of 240 μm and contains 400-μm-wide sense electrodes with 4-μm capacitive gaps stacked on top of each other parallel to the substrate plane. The lateral aspect ratio of the capacitive fingers is currently 100 and can be extended further as far as the stress-induced buckling of the nickel structural layer is small compared to the capacitive-gap spacing. This way, very large capacitance gradients can be achieved by increasing the number of stacked and high aspect-ratio capacitances. The thickness of the proof mass (240 μm) is pretty high compared to its typical silicon counterparts, and, combined with the high material density of nickel (approximately three times higher than silicon), this thickness yields a much lower thermomechanical (Brownian) noise floor at atmospheric pressure compared to that of a silicon gyroscope with similar

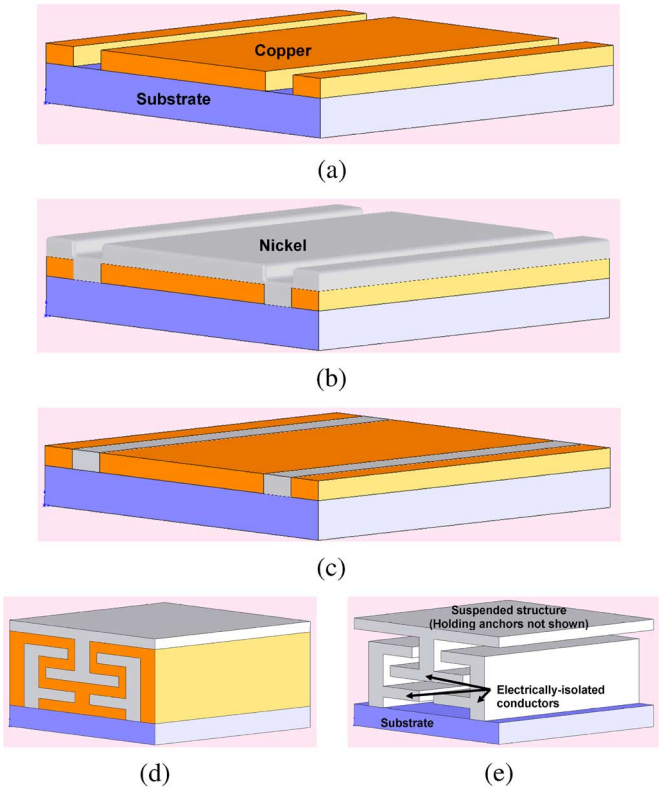

Fig. 4. Illustration of EFAB fabrication process. (a) Electrodeposition of sacrificial copper layer using a patterned hard mask. (b) Electrodeposition of structural nickel on the whole surface. (c) Planarizing the surface. (d) Repetition of steps (a)–(c) for a number of times using different masks. (e) Selective etching of the sacrificial copper layer, releasing the nickel structures.

dimensions. This eliminates the need for vacuum packaging of microgyroscope, making it a suitable candidate for many low-cost gyro applications.

Although the EFAB technology serves significant improvements in the design and realization of truly 3-D microstructures, the designers must be aware of some facts about this process. First of all, the layer-to-layer registration errors of additive electroplated structural layers must be well analyzed; otherwise, it will lead to unexpected device behavior. These errors may increase the bias of the gyroscope. Second, the wire-bonding pads are also implemented by electroplated nickel, which may sometimes be tricky to get electrical connections to the structures. The third fact is the stress gradients of the electroplated nickel. These gradients may cause buckling of thin and lengthy structures and may also be responsible for finite mismatch between in-plane capacitors implemented with this process. Finally, development of vertical-sidewall capacitors is not efficient with this process since the spacing between two neighboring structures cannot be smaller than 10 μm. Still, EFAB process is suitable for generating submillimeter-thick structures with high aspect-ratio in-plane capacitors, which are two important facts that many of the standard micromachining processes cannot compete with.

It should be mentioned here that layer-to-layer registration errors might cause some sidewall roughness in the fabricated structures, and this can affect the symmetry of bulk mass distribution as well as the bending flexures. This effect would

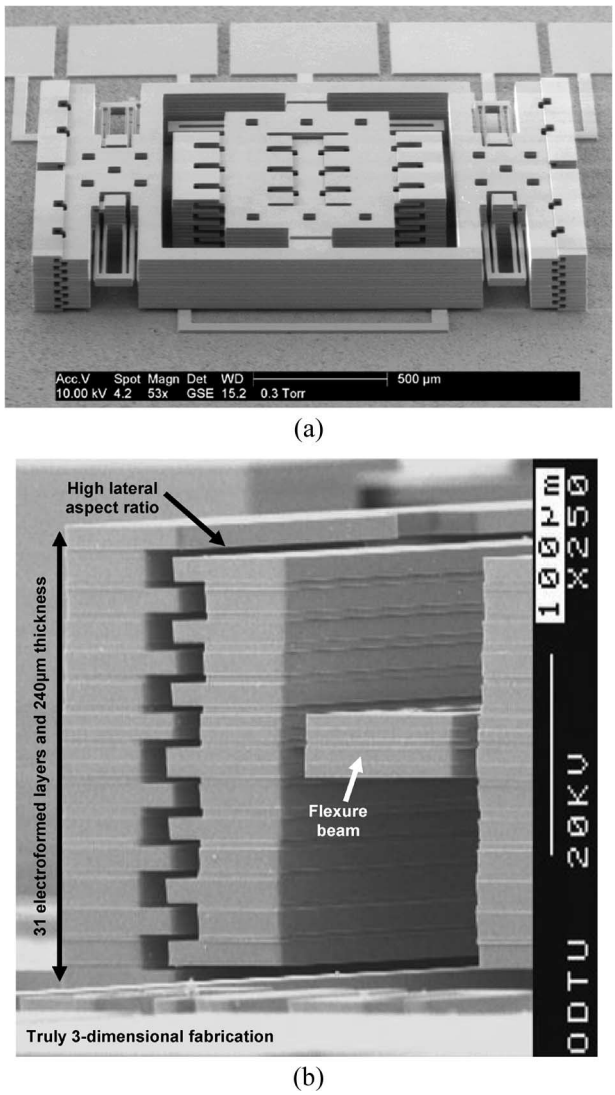

Fig. 5. Fabricated gyroscope consisting of 31 electroformed layers reaching a thickness of 240 μm. The lateral aspect ratio is about 100 and can easily be increased further.

result in a quadrature error, which is measured to be on the order of 600 $^{\circ}/$s for the reported gyroscope. Best efforts do not improve the quadrature error to better than 50 $^{\circ}/$s in silicon sensors even using fully decoupled drive and sense modes. Therefore, the major effort in determining the bias stability of a gyroscope is on the stability of the phase-sensitive demodulation electronics, i.e., on the stability of signal-processing blocks. Therefore, the sidewall roughness in EFAB process causes a nonzero bias error, but the bias stability is still determined by the readout electronics like in the other resonator-based gyroscopes.

IV. Characterization Results

The sensor capacitances and the resonance frequencies associated with the drive and sense modes of the fabricated nickel gyroscope are measured by using the Agilent 4294A precision impedance analyzer and the Agilent 4395A network analyzer, respectively. Differential capacitances of

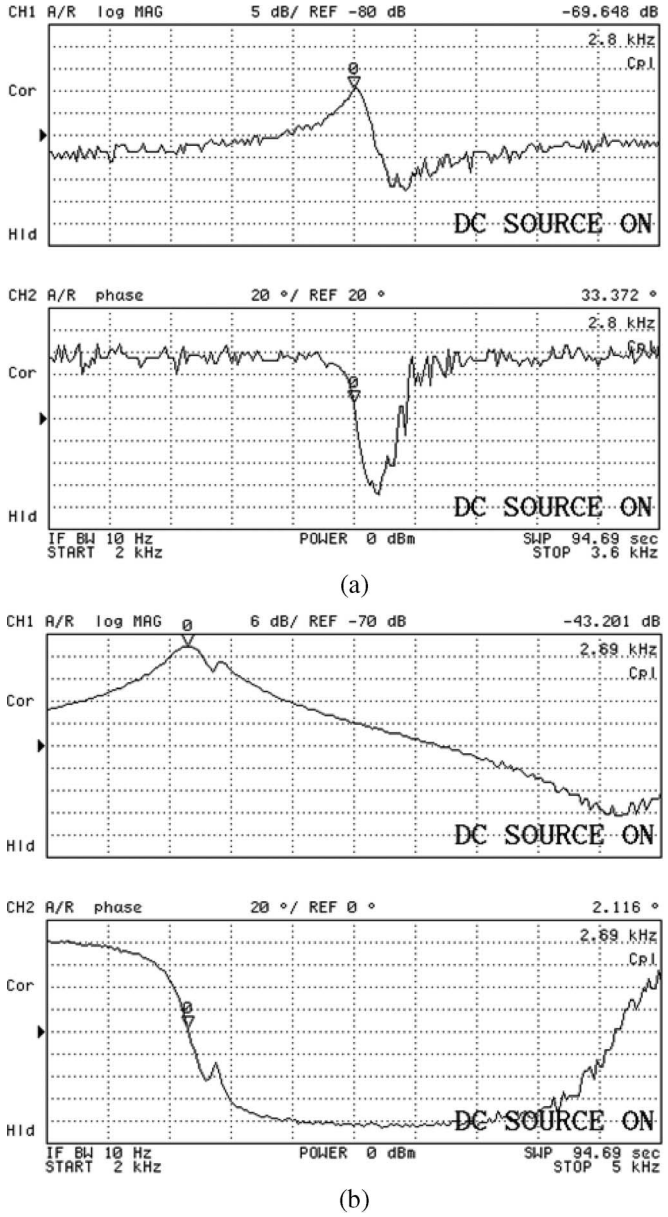

Fig. 6. Measured resonance frequencies of the drive and sense modes at atmospheric pressure and without using a capacitive interface circuit. The drive- and sense-mode frequencies are measured as 2.8 and 2.69 kHz, respectively, including the electrostatic spring effects for a dc polarization voltage of 40 V. Ignoring the electrostatic spring effects, purely mechanical resonance frequency of the sense mode is extracted as 3.65 kHz.

the fabricated gyroscope are measured as 899 and 871 fF for the two drive electrodes and 1481 and 1523 fF for the two sense electrodes. It should be noted here that the amount of mismatch in the differential capacitances of both drive and sense electrodes is quite low. This small mismatch might cause a bias at the output signal but does not degrade the bias stability as the mismatch is expected to remain constant. Fig. 6 shows the resonance frequencies of the drive and sense modes measured at atmospheric pressure and without using a capacitive interface circuit. The drive- and sense-mode pure-mechanical resonance frequencies are measured as 2.8 and 3.65 kHz, respectively, being slightly higher than the design values which is simply due to the layer-thickness tolerance of the fabrication process. Table I presents a comparison of the expected and measured parameters of the fabricated nickel gyroscope. Most of the parameters agree very well with the design values, except for a slight mismatch in the differential sensor capacitances, as a result of stress-induced buckling. Fig. 7 shows the electrostatic tuning of the sense-mode resonance frequency toward the drive-mode frequency in order to enhance the sensitivity of the gyroscope. It is measured that the frequencies of the two modes are closely matched at a dc polarization voltage of 38 V applied to the proof mass. Although this voltage is high for practical applications, it must be mentioned that using smaller polarization voltages (as low as 15 V) does not significantly destroy the mode-matching characteristics, since the sense-mode resonance bandwidth is sufficiently large at atmospheric pressure.

Following the preliminary characterization of the fabricated nickel gyroscope, it is hybrid-connected to a unity-gain buffer-type capacitive interface circuit constructed from LF353 surface-mount operational amplifiers and chip resistors. Fig. 8 shows the schematic of the interface circuit constructed from discrete IC components. The circuit consists of two FET-input buffer amplifiers with 10-MΩ bias resistors biasing the high-impedance input nodes. The output of the drive-mode buffer is also adapted for phase shifting and amplifying the drive-mode output signal and is applied to the drive-mode actuator for the generation of self-resonance along the drive-mode. Fig. 9 shows the fabricated gyroscope sensor chip and the corresponding readout electronics mounted in a 40-pin hybrid package. Fig. 10 shows the measured resonance characteristics of the drive and sense modes using the constructed interface circuit. The measured signal gain at resonance is amplified by a factor of 30 for both modes compared with the measurements in Fig. 7. The total parasitic capacitance associated with the gyroscope sense-mode output node is determined to be above 15 pF, which is dominated by the op-amp preamplifier. This parasitic capacitance significantly reduces the sense-mode output response. Indeed, Fig. 11 shows the measured resonance characteristics of the drive and sense modes using a custom-designed capacitive interface circuit application-specified integrated circuit (ASIC) [17]. Clearly, the response of the gyroscope is amplified by about an order of magnitude, compared to the previous circuit in Fig. 10 when a dedicated CMOS-ASIC is used, as a result of reduced parasitic capacitances. The resonance peaks in Figs. 10 and 11 show slightly different resonance frequencies for the sense mode, mainly due to the disturbing effect of antiresonance dips arising from parasitic feedthrough capacitances. The source of antiresonance dip in Fig. 10 is due to the parasitic capacitances associated with the interface circuit in Fig. 8, which is constructed using discrete IC components. The amount of parasitic capacitances is estimated to be about 15 pF with this circuit. Clearly, the antiresonance dip moves far away in Fig. 11, where a CMOS interface circuit is used, having much smaller parasitic capacitance (< 1 pF). The antiresonance dip is close to the mechanical resonance peak; it adds a disturbance to the overall resonance characteristics.

The CMOS-ASIC that is used in the resonance tests above is suitable for sensors operating at low proof-mass voltages, and it suffers from static-discharge and latch-up

TABLE I
COMPARISON OF THE EXPECTED AND MEASURED PARAMETERS OF THE FABRICATED IN-PLANE GYROSCOPE

	Parameter	Expected	Measured
Drive mode	Mechanical resonance frequency (Hz)	2,515	2,795
	Mechanical spring const. (N/m)	597	737.4
	Quality factor	-	95
	Frequency tuning range (Hz)*	0	0
	Electrode capacitance (fF)	2 x 880	899/871
Sense mode	Mechanical resonance frequency (Hz)	3,491	3,650
	Mechanical spring const. (N/m)	409	447.1
	Quality factor	-	17
	Frequency tuning range (Hz)*	856	750
	Electrode capacitance (fF)	2 x 1505	1481/1523

* For 0 to 40V DC applied to the proof mass

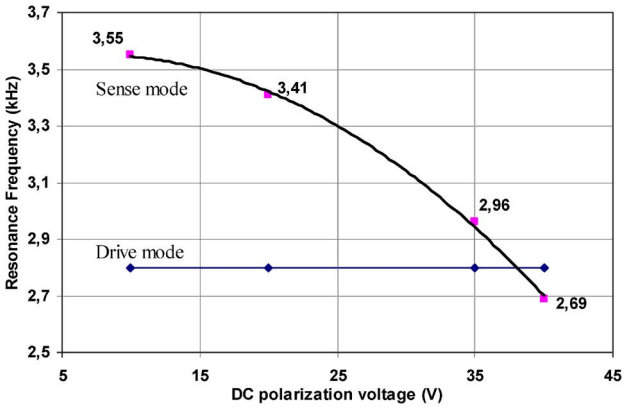

Fig. 7. Electrostatic tuning of the sense-mode resonance frequency toward the drive-mode frequency in order to enhance the sensitivity of the gyroscope. It is measured that the frequencies of the two modes are closely matched at a dc polarization voltage of 38 V applied to the proof mass.

problems when the gyroscope is biased with high dc potentials. Typically, the circuit does not survive throughout the rate tests with a dc voltage sufficient for matching the resonance frequencies of the drive and sense modes. Therefore, the robust interface circuit in Fig. 8, which is constructed from discrete IC components, is used for further characterization of the gyroscope. An improved CMOS-ASIC fabricated in a high-voltage CMOS process would certainly improve the response of the gyroscope, as demonstrated in the resonance measurements.

The gyroscope is entered into self-resonance along the drive mode with a peak oscillation amplitude of about 1 μm. Self-resonance is achieved using a typical positive-feedback oscillator circuit with the gain limited by saturated outputs. Next, the rate sensitivity of the gyroscope is measured using Ideal Aerosmith Model-1280 single-axis rate table. Fig. 12 shows the measured sense-mode output at atmospheric pressure in response to a 2π $^\circ$/s sinusoidal angular-rate input at 20 Hz. The gyroscope demonstrates a measured mechanical sensitivity of 65 μV/($^\circ$/s) and a noise floor of 5.6 μV/Hz$^{1/2}$. The noise equivalent rate is 0.086 $^\circ$/s at atmospheric pressure in a measurement bandwidth of 1 Hz. The high noise at the output of the gyroscope is dominated by the saturation-based positive-feedback-type drive-mode control electronics used to generate self-resonance excitation, the current noise of the 10-MΩ resistors used in biasing the high-impedance input node of the capacitive interface circuit, and the probable process shortcomings. In addition, the noise coupling from the ground reference line and the interfering noise due to off-chip connection of bias resistor also contributes to the total noise. The use of an advanced PI-controller-based self-resonance excitation electronics and a capacitive preamplifier CMOS-ASIC using special biasing techniques such as on-chip subthreshold MOS transistor [11] or on-chip controlled-impedance FET structures [18] can eliminate most of these noise sources. The performance of the gyroscope is currently limited by the quality factor of the sense mode at atmospheric pressure, the large parasitic capacitance, and the high noise from the sensor element as well as the preamplifier and control electronics.

In addition to the rate sensitivity measurements performed at atmospheric pressure, the gyroscope is also evaluated in

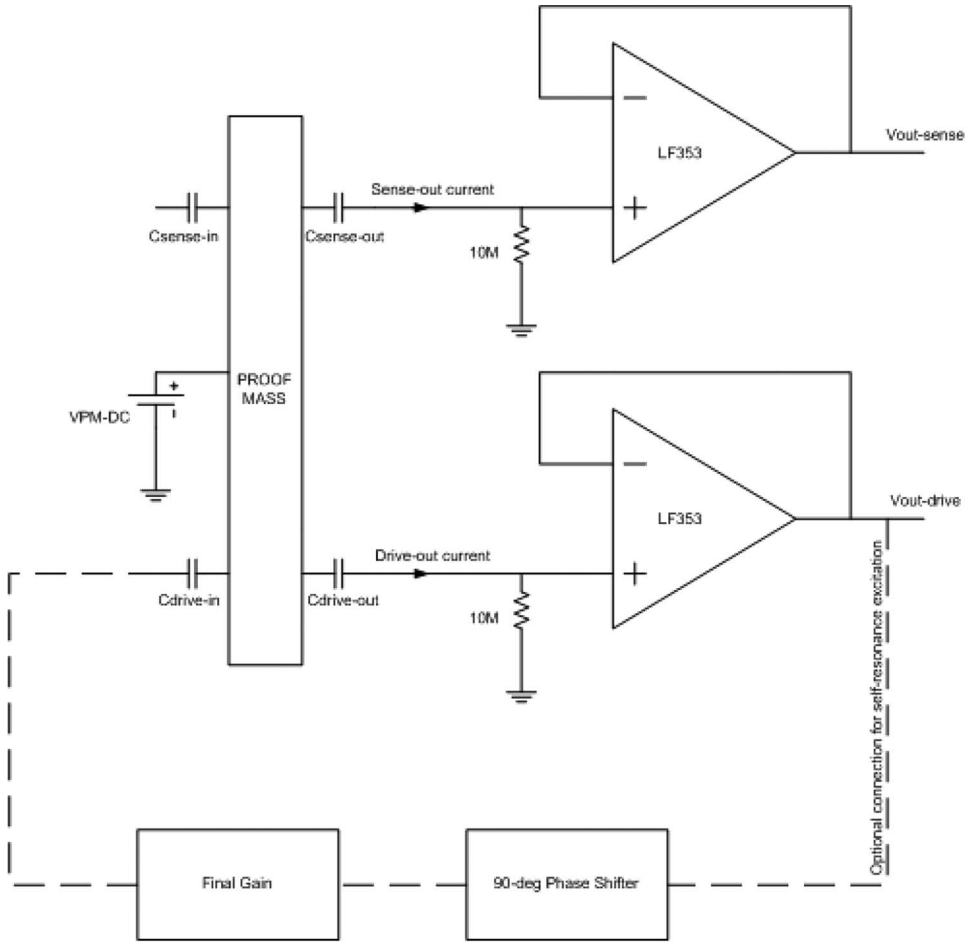

Fig. 8. Schematic view of the interface circuit constructed from discrete IC components.

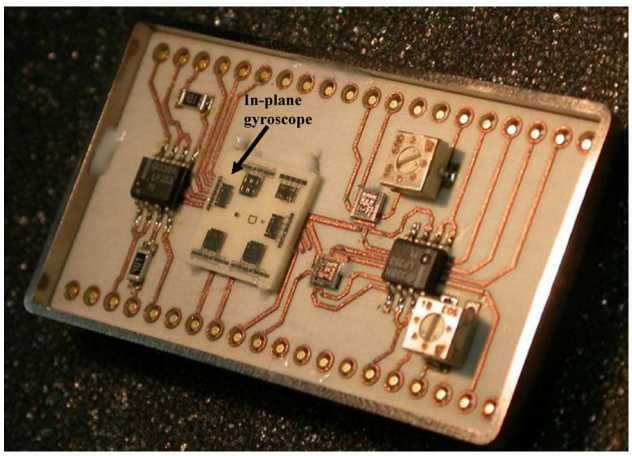

Fig. 9. Fabricated gyroscope sensor chip and the corresponding readout electronics mounted in a 40-pin hybrid package.

a vacuum chamber in order to evaluate the quality of the nickel structural layer and to estimate the ultimate performance limits. Fig. 13 shows the resonance characteristics of the drive and sense modes of the fabricated gyroscope measured at a vacuum level of 20 mtorr. The sense-mode quality factors reach 2000, showing an improvement by more than two orders of magnitude compared to the measured quality factor at atmospheric pressure. It should be noted that high-quality factors can be obtained with electroplated-nickel structures; however, the measured quality factor of the gyroscope reported in this paper is quite good, considering its size, its frequency of operation, and the vacuum level used in the tests. The measured quality factor of the sense mode at vacuum is close to the upper limits reported for electroformed gyroscopes [15] and can significantly further improve the mechanical sensitivity of the gyroscope for applications that require a performance better than 10 °/h, at the expense of vacuum-packaging costs.

The gyroscope presented in this paper is intended to be operated at atmospheric pressure for a high-volume low-cost consumer application. Then, the possible creep of nickel structural material becomes the most important point in questioning the long-term reliability of the gyroscope. Fig. 14 shows drift of the drive-mode resonance frequency at self-resonance for a period of 40 h without any temperature compensation. The variation of the resonance frequency is measured to be less than 0.1%, demonstrating the adequate reliability of the electroformed nickel of the EFAB process. Clearly, the variations in the temperature also affect the resonance frequency of the drive mode, which can be compensated by using calibration of the sensor output in accordance with a temperature sensor.

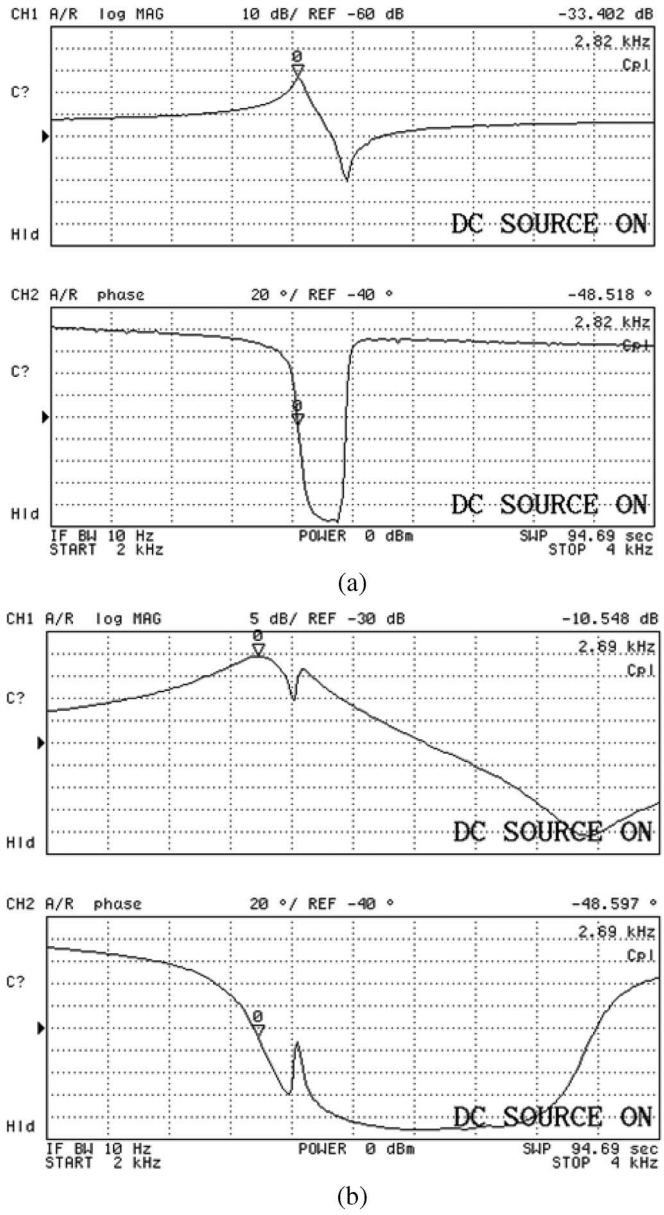

Fig. 10. Measured resonance characteristics of the drive and sense modes using the constructed interface circuit. The measured signal gain at resonance is amplified by a factor of 30 for both modes, compared to the measurements in Fig. 7. The gain is still limited due to high parasitic capacitances (> 15 pF) associated with hybrid electronic components and signal routing.

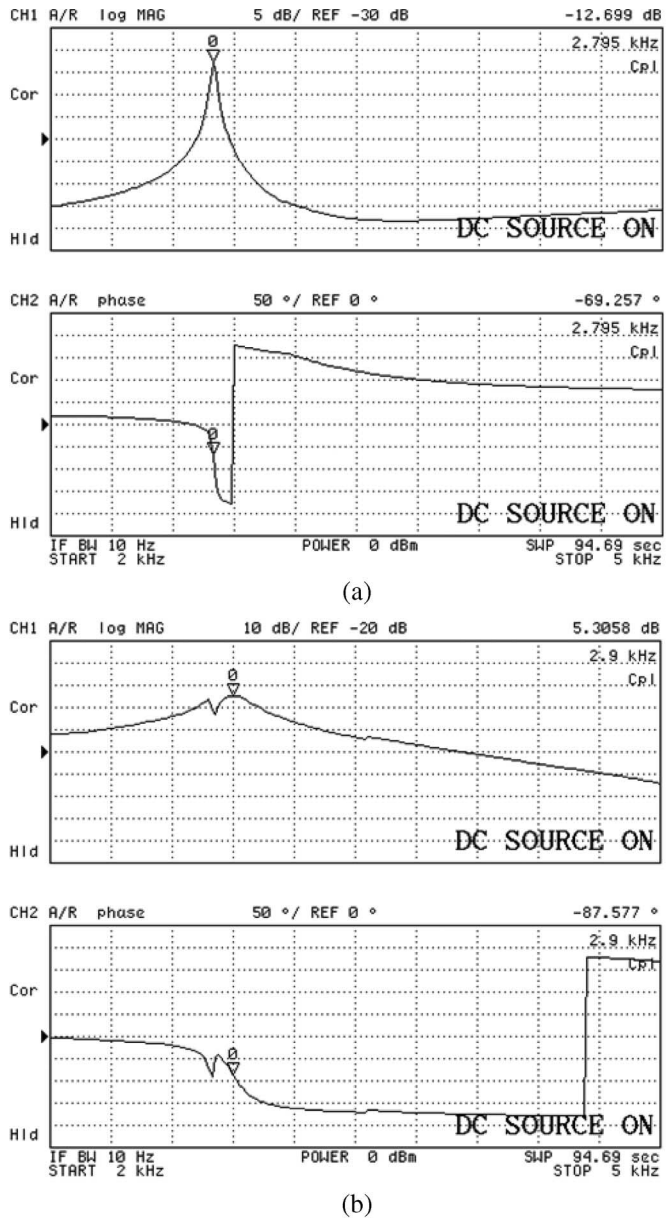

Fig. 11. Measured resonance characteristics of the drive and sense modes using a custom-designed capacitive interface circuit ASIC [17]. Clearly, the response of the gyroscope is amplified by about an order of magnitude compared to the previous circuit in Fig. 10, when a dedicated CMOS-ASIC is used, as a result of reduced parasitic capacitances.

The temperature dependence of the resonance frequencies for the drive and sense modes of the gyroscope is measured, within the temperature range from -40 °C to $+85$ °C, using the temperature chamber of a TENNEY Environmental Test Equipment. The resonance frequencies of the two modes are monitored within the given temperature range and for dc voltages ranging from 10 to 40 V. Fig. 15 shows the plot of the measured resonance frequencies versus the ambient temperature for the drive and sense modes of the gyroscope. The variation of the resonance frequencies of the drive and sense modes with respect to increasing temperature is found to be smaller than 1 and -2 Hz/°C, respectively, in the measurement range from -40 °C to $+85$ °C. Note that the frequency-tuning range of the sense mode is not affected by the ambient temperature as expected. On the other hand, the drive-mode resonance frequency increases as the ambient temperature increases, whereas the sense-mode resonance frequency decreases. This effect must be taken into account during the construction of the temperature-compensation circuit, in order to keep the resonance-frequency matching between the drive and sense modes stable, which is important particularly if the gyroscope is to be operated in a vacuum ambient. Finally, the measured temperature drift characteristics do not contain major deflections from the trend lines in Fig. 15, proving that the gyroscope is suitable for operation in the industrial temperature range with a simple linear temperature-compensation circuit.

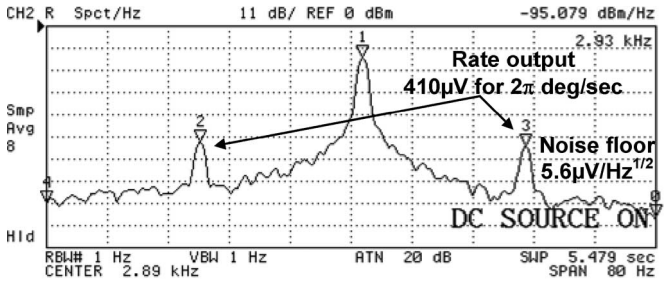

N	SWP PARAM	VAL
0	2.93 kHz	-95.079 dBm/Hz
1	2.891399 kHz	-15.958 dBm/Hz
2	2.87014 kHz	-57.739 dBm/Hz
3	2.912844 kHz	-59.821 dBm/Hz
4	2.85 kHz	-87.958 dBm/Hz

Fig. 12. Measured sense-mode output at atmospheric pressure in response to a 2π $^\circ/$s sinusoidal angular-rate input at 20 Hz. The gyroscope demonstrates a measured mechanical sensitivity of 65 μV/($^\circ$/s) and a noise floor of 5.6 μV/Hz$^{1/2}$.

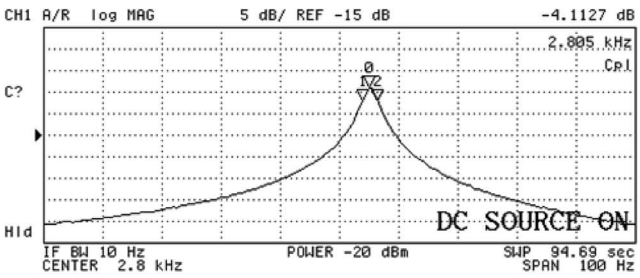

N	SWP PARAM	VAL
0	2.805 kHz	-4.1127 dB
1	2.803775 kHz	-7.1386 dB
2	2.806425 kHz	-7.1873 dB

(a)

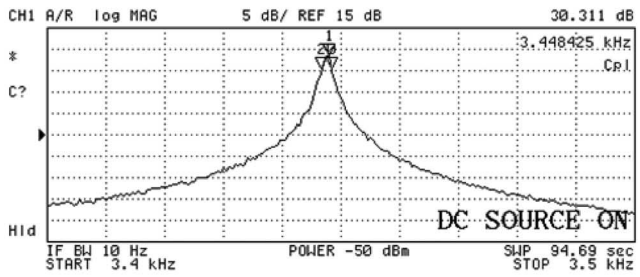

N	SWP PARAM	VAL
0	3.448425 kHz	30.311 dB
1	3.448 kHz	33.411 dB
2	3.4467 kHz	30.381 dB

(b)

Fig. 13. Resonance characteristics of the (a) drive and (b) sense modes of the fabricated gyroscope, which are measured at a vacuum ambient of 25 mtorr and at a 20-V dc polarization voltage applied to the proof mass. Mechanical quality factors are extracted as high as 1100 and 2000 for the drive and sense modes, respectively.

V. Conclusion

This paper has reported on an ultrathick nickel microgyroscope with a lateral aspect ratio greater than 100, which is fabricated using the EFAB commercial multilayer additive electroforming process. The thickness of the structural layer reaches 240 μm by stacking 31 electroplated-nickel layers on top of each other. Ultrathick structural mass yields a lower Brownian noise, even at atmospheric pressure, compared with its silicon counterparts having similar footprint. Furthermore, the sensor capacitances have a lateral aspect ratio of 100, providing a capacitance gradient of 4×10^{-7} F/m even with 4-μm capacitive gap and in a footprint smaller than 3 mm^2. The fabricated gyroscope demonstrates a measured mechanical sensitivity of 65 μV/($^\circ$/s) and a noise equivalent rate of 0.086 $^\circ$/s at atmospheric pressure in a measurement bandwidth of 1 Hz, using a primitive capacitive interface circuit constructed from off-the-shelf components. The measurement bandwidth of the gyroscope is about 100 Hz without using any force-feedback electronics. The performance of the gyroscope at atmospheric pressure is limited by the noise from saturation-based positive-feedback drive-mode control electronics used to generate self-resonance excitation, current noise of preamplifier bias resistors, high parasitic capacitance of the off-the-shelf preamplifier circuit, and low mechanical quality factor of the sense mode due to air-damping effects. It is possible to eliminate these limitations by using advanced control electronics in generating drive-mode self-oscillations, a dedicated CMOS capacitive interface ASIC, and by operating the gyroscope at vacuum ambient. The gyroscope demonstrates quality factors reaching 2000 at 20-mtorr vacuum

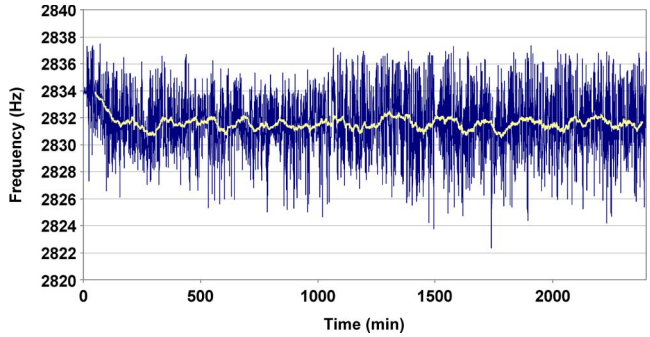

Fig. 14. Drift of the drive-mode resonance frequency at self-resonance for a period of 40 h, without using any temperature control. The variation of the resonance frequency is measured to be less than 0.1%, demonstrating the reliability of the electroformed nickel of the EFAB process.

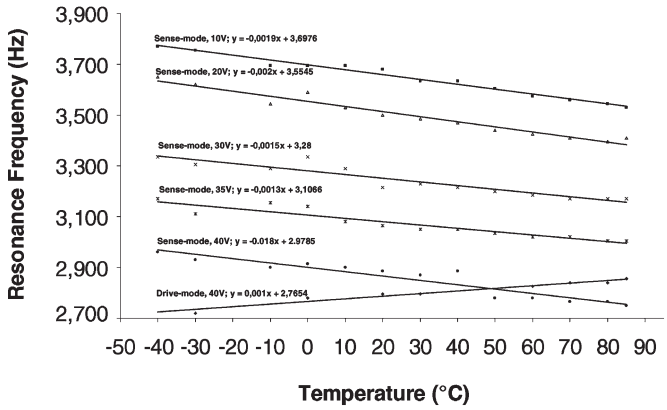

Fig. 15. Measured resonance frequencies versus ambient temperature for the drive and sense modes of the fabricated gyroscope.

ambient, approximately two orders of magnitude higher than that measured at atmospheric pressure demonstrating the quality of the structural nickel layer. Another indication showing the quality of the nickel structural layer is the stability of drive-mode resonator of the gyroscope. The variation of the drive-mode resonance frequency is measured to be better than 0.1% within the 40-h period, demonstrating the reliability of the electroformed nickel of the EFAB process. The resonance frequencies of both the drive and the sense modes are also characterized against temperature variations, and their variation with increasing temperature is measured to be smaller than 1 and -2 Hz/°C, respectively, in a measurement range from -40 °C to $+85$ °C.

Although the characterized performance is demonstrative about the ultimate performance of the EFAB gyroscope, still, there is a path for further improvements. The reliability and performance of the gyroscope can be improved by using some advanced alloys of nickel that can provide better mechanical properties, which are under development by Microfabrica, Inc. The rate sensitivity of the gyroscope would certainly improve by using a CMOS preamplifier instead of one with discrete IC components. In addition, it is necessary to construct high-quality phase-sensitive detection electronics at the output of this gyroscope in order to estimate the bias drift and related performance criteria. The gyroscope performance can be further improved by using a temperature-compensation circuit for compensating the effects of gas-damping variations with ambient temperature at atmospheric pressure. The sensitivity of the gyroscope is estimated to be improved by an order of magnitude approaching 0.01 °/s at atmospheric pressure, with the use of a low-noise and high input-impedance CMOS capacitive interface ASIC. The demonstrated performance of the fabricated gyroscope at atmospheric pressure and the CMOS-compatible nature of the fabrication process make this gyroscope a candidate particularly for applications requiring low cost yet high performance, without a need for vacuum packaging.

ACKNOWLEDGMENT

The authors would like to thank V. Arat and Dr. C. Bang from Microfabrica, Inc., for their help in fabrication, and K. M. Silay for his efforts during the tests of the fabricated gyroscope.

REFERENCES

[1] G. He and K. Najafi, "A single-crystal silicon vibrating ring gyroscope," in *Proc. IEEE MEMS Workshop*, Las Vegas, NV, Jan. 2002, pp. 718–721.

[2] F. Ayazi and K. Najafi, "A HARPSS polysilicon vibrating ring gyroscope," *J. Microelectromech. Syst.*, vol. 10, no. 2, pp. 169–179, Jun. 2001.

[3] S. E. Alper and T. Akin, "A single-crystal silicon symmetrical and decoupled gyroscope on insulating substrate," in *Proc. 12th Int. Conf. Transducers*, Jun. 2003, pp. 1399–1402.

[4] K. Y. Park, H. S. Jeong, S. An, S. H. Shin, and C. W. Lee, "Lateral gyroscope suspended by two gimbals through high aspect ratio ICP etching," in *Proc. 10th Int. Conf. Transducers*, Jun. 1999, pp. 972–975.

[5] W. Geiger, W. U. Butt, A. Gaißer, J. Frech, M. Braxmaier, T. Link, A. Kohne, P. Nommensen, H. Sandmaier, and W. Lang, "Decoupled microgyros and the design principle DAVED," *Sens. Actuators A, Phys.*, vol. 95, no. 2/3, pp. 239–249, Jan. 2002.

[6] N. Hedenstierna, S. Habibi, S. M. Nilsen, T. Kvisteroy, and G. U. Jensen, "Bulk micromachined angular rate sensor based on the butterfly-gyro structure," in *Tech. Dig. IEEE MEMS Conf.*, Interlaken, Switzerland, Jan. 2001, pp. 178–181.

[7] H. Kawai, K.-I. Atsuchi, M. Tamura, and K. Ohwada, "High-resolution microgyroscope using vibratory motion adjustment technology," *Sens. Actuators A, Phys.*, vol. 90, no. 1/2, pp. 153–159, May 2001.

[8] N. Yazdi and K. Najafi, "An all-silicon single-wafer micro-g accelerometer with a combined surface and bulk micromachining process," *J. Microelectromech. Syst.*, vol. 9, no. 4, pp. 544–550, Dec. 2000.

[9] J. Bernstein, S. Cho, A. T. King, A. Kourepenis, P. Maciel, and M. Weinberg, "A micromachined comb-drive tuning fork rate gyroscope," in *Proc. IEEE MEMS Workshop*, Fort Lauderdale, FL, Feb. 1993, pp. 143–148.

[10] S. Chang, M. Chia, P. Castillo-Borelley, W. Hidgon, Q. Jiang, J. Johnson, L. Obedier, M. Putty, Q. Shi, D. Sparks, and S. Zarabadi, "An electroformed CMOS integrated angular rate sensor," *Sens. Actuators A, Phys.*, vol. 66, no. 1–3, pp. 138–143, Apr. 1998.

[11] S. E. Alper, K. M. Silay, and T. Akin, "A low-cost rate-grade nickel microgyroscope," *Sens. Actuators A, Phys.*, vol. 132, no. 1, pp. 171–181, Nov. 2006.

[12] K. Schumacher, O. Kromer, U. Wallrabe, J. Mohr, and V. Saile, "Micromechanical-LIGA gyroscope," in *Tech. Dig. 10th Int. Conf. TRANSDUCERS*, Sendai, Japan, Jun. 1999, pp. 1574–1577.

[13] S. E. Alper, I. E. Ocak, and T. Akin, "Ultra-thick and high-aspect-ratio nickel microgyroscope using EFAB multi-layer additive electroforming," in *Proc. 19th IEEE Int. Conf. MEMS*, Istanbul, Turkey, Jan. 2006, pp. 670–673.

[14] W. C. Tang, M. G. Lim, and R. T. Howe, "Electrostatic comb drive levitation and control method," *J. Microelectromech. Syst.*, vol. 1, no. 4, pp. 170–178, Dec. 1992.

[15] D. R. Sparks, M. I. Chia, and G. Q. Jiang, "Cyclic fatigue and creep of electroformed micromachines," *Sens. Actuators A, Phys.*, vol. 95, no. 1, pp. 61–68, Dec. 2001.

[16] [Online]. Available: www.microfabrica.com

[17] S. E. Alper and T. Akin, "A symmetrical and decoupled nickel microgyroscope on insulating substrate," *Sens. Actuators A, Phys.*, vol. 115, no. 2/3, pp. 336–350, Sep. 2004.

[18] J. A. Geen, S. J. Sherman, J. F. Chang, and S. R. Lewis, "Single-chip surface micromachined integrated gyroscope with 50°/h Allan deviation," *J. Solid-State Circuits*, vol. 37, no. 12, pp. 1860–1866, Dec. 2002.

Said Emre Alper was born in Ankara, Turkey, in 1976. He received the B.S., M.S., and Ph.D. degrees in electrical and electronics engineering (with high honors) from the Middle East Technical University (METU), Ankara, in 1998, 2000, and 2005, respectively.

From 1998 to 2005, he was a Research Assistant with the MEMS-Very Large Scale Integration Research Group, Department of Electrical and Electronics Engineering, METU, where he has been a Senior Research Scientist since 2006. His major research interests include capacitive inertial sensors, micromachined resonators and actuators, capacitive interface circuits, and microfabrication technologies.

Dr. Alper received the "METU Thesis of the Year Award" in 2000 and 2005 for his M.Sc. thesis and Ph.D. dissertation, respectively, which were awarded by the Prof. Mustafa N. Parlar Education and Research Foundation. He is the first author of the symmetric and decoupled gyroscope design, which won the first-prize award in the operational designs category of the "International Design Contest" organized by Design, Automation, and Test in Europe and CMP in March 2001. He is also the first author of the tactical-grade symmetrical and decoupled microgyroscope design, which won the third-prize award, among 132 MEMS designs from 24 countries and 25 states across the U.S., in the international "3-D MEMS Design Challenge" organized by MEMGEN Corporation (currently Microfabrica, Inc.) in June 2003.

Ilker Ender Ocak was born in Ankara, Turkey, in 1981. He received the B.S. degree in electrical engineering with a minor in mechatronics engineering (with honors) from the Middle East Technical University (METU), Ankara, in 2003, where he is currently working toward the Ph.D. degree.

He is also currently a Research Assistant with METU. His major research interests include capacitive inertial sensors, inertial measurement units, micromachined resonators and actuators, microfabrication technologies, and analog and digital integrated circuits.

Tayfun Akin (S'90–M'97) was born in Van, Turkey, in 1966. He received the B.S. degree in electrical engineering (with high honors) from the Middle East Technical University (METU), Ankara, Turkey, in 1987. He moved to the USA in 1987 for his graduate studies with a graduate fellowship provided by the North Atlantic Treaty Organization Science Scholarship Program through the Scientific and Technical Research Council of Turkey. He received the M.S. and Ph.D. degrees in electrical engineering from the University of Michigan, Ann Arbor, in 1989 and 1994, respectively.

In 1995 and 1998, he was an Assistant Professor and an Associate Professor, respectively, with the Department of Electrical and Electronics Engineering, METU, where he has been a Professor since 2004. He is also the Technical Coordinator of METU-Microelectronic Technologies, which is an IC fabrication factory which was transferred to METU by the government for MEMS-related production. His research interests include MEMS, microsystems technologies, infrared detectors and readout circuits, silicon-based integrated sensors and transducers, and analog and digital integrated-circuit design.

Dr. Akin has served in various MEMS, EUROSENSORS, and TRANSDUCERS conferences as a Technical Program Committee Member. He was the Cochair of the 19th IEEE International Conference of Micro Electro Mechanical Systems (MEMS 2006) held in Istanbul. He was the recipient of the first-prize award in experienced analog/digital mixed-signal design category at the 1994 Student VLSI Circuit Design Contest organized and sponsored by Mentor Graphics, Texas Instruments, Hewlett–Packard, Sun Microsystems, and *Electronic Design Magazine*. He is the coauthor of the symmetric and decoupled gyroscope project which won the first-prize award in the operational designs category of the International Design Contest organized by the Data Automation and Test in Europe Conference and CMP in March 2001. He is also the coauthor of the gyroscope project which won the third-prize award of the 3-D MEMS Design Challenge organized by MEMGEN Corporation (currently Microfabrica, Inc.).